Contents lists available at ScienceDirect

Chemical Engineering Journal

journal homepage: http://ees.elsevier.com

# $No_x$ emission performance assessment on a perforated plate-implemented premixed ammonia-oxygen micro-combustion system

Tao Cai [a], Sid M. Becker [a], Feng Cao [a], Bing Wang [b], Aikun Tang [c], Jianqin Fu [d], Lei Han [a,e], Yuze Sun [a], Dan Zhao [a,*]

[a] Department of Mechanical Engineering, College of Engineering, University of Canterbury, Private Bag 4800, Christchurch 8140, New Zealand
[b] School of Aerospace Engineering, Tsinghua University, Beijing 100084, China
[c] School of Energy and Power Engineering, Jiangsu University, Zhenjiang 212013, China
[d] State Key Laboratory of Advanced Design and Manufacturing for Vehicle Body, Hunan University, Changsha 410082, China
[e] School of Aerospace Engineering, Beijing Institute of Technology, Beijing 100083, China

ARTICLE INFO

*Keywords*
Ammonia
Perforated plate
$NO_x$ emission
Flow field
Conjugate heat transfer
Preferential diffusion

ABSTRACT

The present work examines the $NO_x$ emission characteristics of a premixed micro-combustion system with a perforated plate implemented. For this, a three-dimensional (3D) computational model involving a detailed chemical-kinetic mechanism for ammonia-oxygen combustion in the micro-combustor is developed. The model is first validated with the experimental measurements available in the literature before conducting comprehensive analyses. It is found that implementing a perforated plate in the micro-combustion system creates a flow recirculation zone downstream characterized by a low flame temperature and combustion speed. Meanwhile, the conjugate heat transfer between the combustion products and the inner combustor walls is shown to play a key role in the NO generation by relocating the flame in the axial direction and thus changing the chemical reaction rate. Furthermore, the preferential diffusion caused by the variation in the mass diffusivity of different species and the two-dimensionality flow is identified to vary significantly in comparison with the case in the absence of the perforated plate, especially in the vicinity of the recirculation zone. This diffusion effect results in the considerable drop in the N/O atomic ratio, primarily due to the reduction and increase of $O_2$ and $H_2O$, together with less available $N_2$, and consequently affecting the NO generation rate. This work confirms that the flow field, the conjugate heat transfer as well as the preferential diffusion effect could be regarded as the potential mechanisms leading to the $NO_x$ emission variation in the recirculation zones.

**Nomenclature**

3D
three-dimensional
$C_p$
specific heat of species, J/kg· K
CO
carbon monoxide
$CO_2$
carbon dioxide
$CH_4$
methane
$D$
characteristic length, m
$h$
convection heat transfer coefficient, $W/m^2/·K$
$H$
combustor height, m
$H_2$
hydrogen
$H_2O$
water
$k$
thermal conductivity of species, W/m/·K
$L$
combustor length, mm
$NH_3$
ammonia
NO
nitric oxide
$NO_x$
nitric oxides

* Corresponding author.
*E-mail address:* dan.zhao@canterbury.ac.nz (D. Zhao)

https://doi.org/10.1016/j.cej.2020.128033
Received 13 August 2020; Received in revised form 2 December 2020; Accepted 4 December 2020
Available online xxx
1385-8947/

$N_2O$
nitrous oxide
$NO_2$
nitrogen dioxide
$N_2$
nitrogen
$O_2$
oxygen
OH
hydroxyl radical
OWT
outer wall temperature, K
Pe
Peclet number
PP
perforated plate
$q$
heat loss rate, W/m$^2$
RR
reduction ratio
SIMPLE
semi-implicit method for pressure linked equations
$t$
wall thickness, mm
$T_W$
temperature of the combustor outer wall, K
$T_\infty$
ambient temperature, K
$u$
fluid velocity, m/s
$W$
combustor width, mm
$x, y, z$
rectangular coordinates, mm
$X_i$
mole fraction of species $i$
$X_{wo}$
NO mole fraction without a perforated plate
$X_{wt}$
NO mole fraction with a perforated plate

**Greek symbols**

$\rho$
fluid density, kg/m$^3$
$\varepsilon$
solid emissivity
$\sigma$
Stephan-Boltzmann constant, W/m$^2$/K$^4$
$\phi$
initial fuel-oxidizer equivalence ratio
$\phi_{local}$
local equivalence ratio

$\phi_{local} - \phi$
departure of local equivalence ratio from the initial one
$\Delta x$
distance away from the downstream face of the perforated plate in the streamwise direction, mm
$\gamma_{N/H}$
local nitrogen-to-hydrogen atomic ratio
$\gamma_{N/O}$
local nitrogen-to-oxygen atomic ratio

## 1. Introduction

Global concerns with climate change, energy sustainability and availability have triggered a wide research interest in seeking alternative fuels to replace hydrocarbon fossil fuels. Some potential energy vectors, such as hydrogen ($H_2$) and ammonia ($NH_3$), are being explored, and considered to play a positive role in addressing these issues [1–3]. Concerning these two fuels, $H_2$ is considered as the first option as it does not contain any carbons and the only combustion product is water ($H_2O$), thus eliminating some undesirable emissions. However, there are some technical and economic challenges associated with $H_2$ usage. These includes the storage, transportation, and hard controlling, because of the high reactivity and burning velocity [4]. It is acknowledged that $H_2$ has a high volatility and low flash point, and is likely to be more explosive compared to $NH_3$. It has a high hydrogen content and carbon-free characteristics [5]. In addition, $NH_3$ has a well-established global production and transportation infrastructure [6], indicating that it is more cost-effective to transport this fuel than that of $H_2$. Accordingly, $NH_3$ may be more suitable for storage and transportation in current infrastructures. Despite the cost challenges associated with $NH_3$ synthesis, some net-zero-energy eco-friendly ways to minimize the production cost have been proposed and tested by utilizing renewable energy sources, such as wind and solar energy [7,8]. Finally, there are no carbon dioxide-involved emissions when combusting $NH_3$. In light of these attractive features above, $NH_3$ has the potential to play an influential role in the power generation and propulsion systems as a sustainable and renewable fuel.

Before ammonia being applied in practice, it is of particular importance to gain a comprehensive understanding of the fundamental physical and chemical characteristics of $NH_3$ combustion. Typically, there are two major challenges that need to be addressed for burning $NH_3$. The first one is how to promote flame stability resulting from the relatively lower laminar burning velocity in comparison to $H_2$ and hydrocarbon fuels. In an effort to tackle this issue, extensive research has been conducted specifically designed to enhance the ammonia-involved flame speed or extend the mixture residence time. These are mainly focused on the inlet operating parameter, combustion chamber structure as well as binary fuels [5,9]. Liu et al. [10] conducted experimental and numerical studies on the laminar flame speed of ammonia/oxygen combustion. Their results showed that the laminar flame speed reached its peak value under the stoichiometric condition with an initial pressure of 0.5 atm. Hayakawa et al. [11] experimentally evaluated the flame speed of a premixed ammonia/air with varied inlet pressure. The flame speed was identified to increase as decreasing the inlet pressure. The effect of the radiation heat loss on the burning velocity of laminar ammonia/air premixed flames was examined [12] using Chemkin-Pro 17.2. The flame speed was found to be strongly affected by the radiation heat loss over a wide range of equivalence ratio. In addition, Hayakawa et al. [13] experimentally demonstrated the stable combustion of ammonia/air by introducing a swirler and thus extending the flame residence time within the combustor. Furthermore, fuel composition is also proven to have a significant impact on the flame velocity of the mixture. The effects of methane and hydrogen addition in swirl-assisted gas turbine combustors were assessed by Xiao et al. [14] and Valera-Medina et al. [15,16] by applying experimental and numerical approaches. It was demonstrated that adding a high mass diffusivity fuel to ammonia could significantly elevate the flame burning velocity and thus promote the flame stability.

Another issue associated with using ammonia is the high $NO_x$ emissions, which are the main precursors of smog and acid rain that are harmful to both the environment as well as human being health [17–19]. Hence, a number of analytical, numerical, and experimental studies have been conducted, with the emphasis being placed on reduc-

ing $NO_x$ formation [20,21]. Li et al. [5] experimentally and numerically evaluated the $NO_x$ emissions of $H_2$-$NH_3$-air combustion. Thermal-$NO_x$ was found to be decreased when adding $NH_3$ to $H_2$, primarily due to the low flame temperature of $NH_3$. Xiao et al. [14] demonstrated that blending $NH_3$ to $CH_4$ can enable the CO and $CO_2$ emissions being reduced with a high NO emission. Somarathne et al. [22] compared the emission characteristics of ammonia/air and methane/air flames. It was found that regarding $NH_3$ /air flames, the local NO concentration highly depended on the local OH concentration, whereas for $CH_4$/air flames, the local NO concentration was primarily dependent on the local flame temperature. NO formation was identified to be strongly sensitive to the inlet pressure, and a low NO emission can be achieved with a high inlet pressure [23,24]. Okafor et al. [17] discovered that compared to ammonia non-premixed combustion, its counterpart premixed one tended to give a low $NO_x$ emission. In their follow-up work, experimental and numerical investigations on the emission performance of ammonia-methane-air in a micro gas turbine combustor were implemented [25]. It was found that the optimum equivalence ratio, where $NO_x$ emission was lower, was found to vary from 1.30 to 1.35 depending on the $NH_3$ concentration. Special configurations have been applied to the combustion chamber for realization of a low emission. Meyer et al. [26] identified that the implementation of a flame holder was capable of reducing $NO_x$ emissions with a increased combustion efficicency. Somarathne et al. [27] highlighted that at a high pressure, ammonia swirl flame can be involved with a low emission in the presence of a secondary air injection.

To the best knowledge of the present authors, there is little work in the literature analyzing the perforated plate effect on $NO_x$ formation in an ammonia-fuelled micro-power system. This partially motivated the present work. In this work, we attempt to explore the $NO_x$ emission characteristics in a perforated plate-implemented micro-power system. Thus it can provide insights into the effects of the flame-flow, the flame-wall interaction due to the conjugate heat transfer between the combustion products and the inner walls, and the preferential diffusion caused by different mass diffusivities of species. In Section 2, the physical and computational models are presented. Analyses of mesh independence and chemical reaction mechanisms are conducted. The numerical model is validated by comparing the present numerical and experimentally measured results. In Section 3, the impact of implementing a perforated plate on the $NO_x$ formation is qualitatively and quantitatively evaluated. Detailed assessments on the $NO_x$ emissions are discussed in terms of the flow field, the conjugate heat transfer, and the preferential diffusion effect. Finally, in Section 4, key concluding remarks are summarized.

## 2. Numerical methodology

### 2.1. Geometric model

In this work, we consider applying a perforated plate with a rectangular-shaped orifice in a micro-combustion system to investigate its effect on $NO_x$ generation by shedding lights on the fundamental mechanisms. This is different from the previous work [28], where a conventional rectangular micro-combustor without any blocking device confined is studied. Such micro-combustor with a perforated plate applied is schematically presented in Fig. 1. The overall geometries of the micro-combustor is 20 mm length $L$, 11 mm width $W$, and 3 mm height $H$, with the thickness $t$ of all the walls being set to 0.5 mm. As a result, the channel width and height of the combustor are 10 mm and 2 mm respectively. The upstream surface of the perforated plate is located at an axial distance of 8 mm away from the combustor inlet, while the width and height of the plate hole are 5 mm and 1 mm, respectively. In such way, the aspect ratio of the perforated plate hole is the same as that of the combustor inlet. In addition, the thickness $t_1$ of the perforated plate is 1 mm. The solid material is assumed to be made of steel, unless otherwise noted.

### 2.2. 3D computational model

In this work, ANSYS (Fluent 18.1) is selected as the computational tool to systematically solve all the governing equations associated with the coupled flow-combustion-heat/mass transfer-thermodynamics. These governing equations include the mass continuity, momentum, energy and species. The combustion for premixed ammonia/oxygen is modeled using a detailed kinetics mechanism involving 22 species and 67 reactions [29]. The pressure-velocity is decoupled employing SIMPLE (Semi-Implicit Method for Pressure Linked Equations) algorithm. The second-order upwind scheme is adopted to discretize all the equations and species, with convergence criteria for all residuals being set to be less than $10^{-6}$.

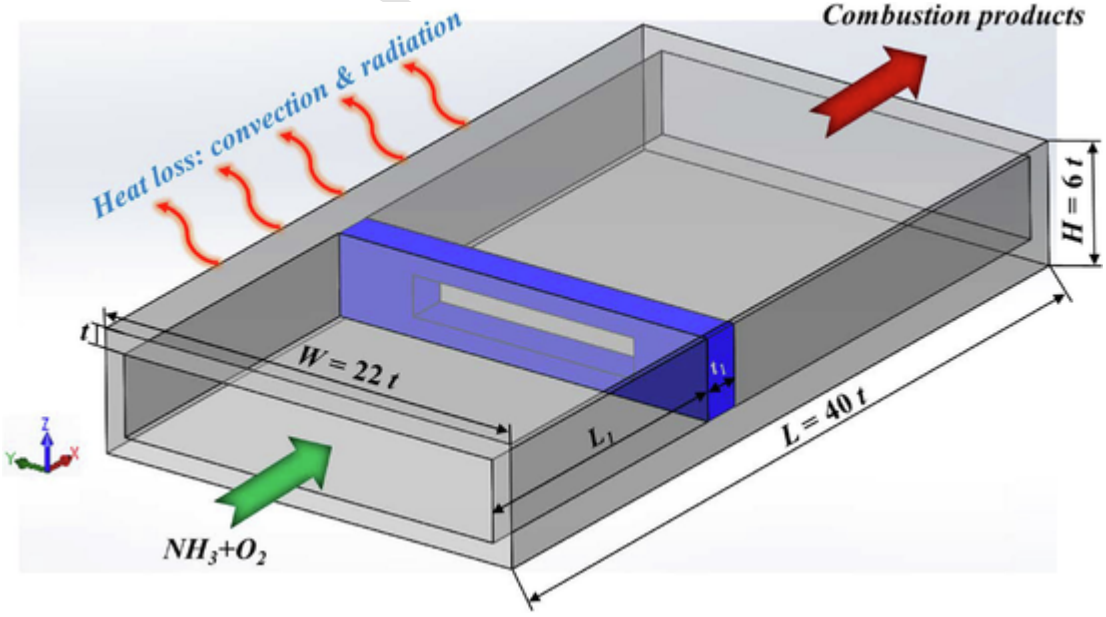


**Fig. 1.** Schematic of the modified micro-planar combustor with a perforated plate.

The maximum Reynolds number on the basis of the mixture inlet velocity and the area of the combustor inlet is less than 500. Consequently, modeling of laminar for the fluid flow is considered [30], while the chemical reaction is modeled using the finite rate model. With regard to the fuel-oxidizer mixture properties, the thermal conductivity and viscosity are calculated by the ideal-gas-mixing law, while the specific heat is obtained according to the mixing-law [31]. When it comes to an individual species, the specific heat is computed based on a piecewise polynomial fit of temperature, while the thermal conductivity and viscosity are calculated via the kinetic-theory [31]. The gas radiation model is included to boost the accuracy of computational results [32]. As for the Soret and Dufour effects, the former one is shown to play a critical role in NO production, and thus is included in the present simulation. However, the latter one has little influence on the combustion process, and therefore is neglected [33,34]. Furthermore, the effect of the pressure diffusion is not considered because of the small magnitude [35,36]. As for the settings of the Fluent model, the $NO_x$ model provides the capability to model thermal, prompt, and fuel $NO_x$ formation, as well as $NO_x$ consumption due to re-burning in combustion systems. In view of the fact that there is no re-burning combustion considered in this work, and fuel-$NO_x$ has a dominant role when modelling ammonia oxidation, while thermal-$NO_x$ and prompt-$NO_x$ have negligible roles [5]. Thus $NO_x$ model is neglected in all present calculations. The computed NO is primarily from fuel-nitrogen combustion, irrespective of whether the $NO_x$ model is applied or not. As far as $NO_x$ emissions are concerned, there are steps involving the formation and destruction of nitrogen dioxide ($NO_2$), nitrous oxide ($N_2O$), and NO. However, $NO_2$ and $N_2O$ formation from these steps are found to play a negligible role in the total $NO_x$ emissions compared to NO formation. Thus NO emissions will be considered as the indicator of the total emissions for simplification. This was experimentally and numerically demonstrated in previous studies [37,38].

The boundary conditions are specified as follows. For the channel inlet, a uniform velocity profile with an initial pressure of 1 atm and temperate of 300 K is assumed. With respect to the channel outlet, the pressure-outlet boundary is modelled. All the external walls are modeled using mixed thermal conditions involving the radiation and convection heat transfer [39,40]. Therefore, the formulation for calculating the heat loss rate between the combustor out wall and the atmosphere can be written as:

$$q = h\left(T_W - T_\infty\right) + \varepsilon\sigma\left(T_W^4 + T_\infty^4\right) \quad (1)$$

where $h$ is the convection heat transfer coefficient (20 W/(m$^2$/·K)); $T_W$ is the temperature of the combustor outer wall; $T_\infty$ represents the ambient temperature (300 $K$); $\varepsilon$ represents the solid emissivity (0.85 [41,42]);$\sigma$ denotes the Stephan-Boltzmann constant ($5.67 \times 10^{-8}$ W/(m$^2$/·K$^4$)).

### 2.3. Grid independence and reaction mechanisms comparison

To obtain good computational results without causing high computational expense, the grid-independence analysis is conducted using three sets of grid resolutions. Mesh generation is performed via Gambit 2.4.6. In the present work, the fuel/oxidizer ratio is assumed to be 1.0, unless otherwise specified. Fig. 2 presents the comparison of profiles for centerline temperature and OH mole fraction on the cross section along the axial direction with the grid resolution with the $NH_3$ volumetric flow rate of 400 mL/min. Fig. 2 (a) shows good agreements of temperature profiles between the medium and fine mesh in terms of the peak value and its location. However, a considerable deviation is found to take place between the coarse and medium mesh. From Fig. 2 (b), it can be noted that there is a negligible difference in the OH profiles, no matter which mesh size is set to. A comparison of Fig. 2 (a) and (b) demonstrates that the medium grid resolution is sufficient to accurately capture the combustion characteristics.

In numerical simulations, it is preferable to apply a reaction mechanism with a much more detailed chemistry and species transport, but it could lead to a prohibitive amount of computational cost. Hence, the use of a simplified kinetic mechanism capable of capturing the basic combustion characteristics is more realistic and desirable. Therefore, the calculated results from the mechanism developed by Drake and Blint [29] are first compared with those obtained by using the mechanism proposed by Nakamura et al. [43]. The latter one involves 38 elementary species and 232 steps, and has been identified to be applicable under micro-scale conditions. Fig. 3 compares the outer wall temperature (OWT) and the NO concentration at the combustor outlet with two different kinetic mechanisms, as the $NH_3$ volumetric flow rate is set to 4 different values. It can be seen that there is a good agreement in the OWT obtained with different reaction mechanisms, with the maximum relative error being 1.3%. Meanwhile, NO production rates also have a similar trend. Accordingly, it can be concluded that the present detailed reaction mechanism is sufficiently reliable to simulate ammonia flames.

### 2.4. Validation of numerical model

To confirm the accuracy of the numerical model, the computed axial temperatures on the outer wall of the combustor for methane flames are examined and compared with experimentally measured data in Ref. [44], due to the absence of experimental ammonia data that occur under micro-scale conditions. Fig. 4 presents the profiles of methane/air and ammonia/oxygen flames at two different inlet velocities, with the ratio of fuel to oxidizer being set to 1.0. It can be clearly seen that as far as methane/air flames are concerned, there is a good agreement between the experimental and predicted results in terms of the temperature shape. The maximum relative error is found to be 5.1% with the inlet velocity of 0.6 m/s. It is, however, worthwhile to mention that there are some differences in the temperature profiles in methane and ammonia flames. This is quite understandable because the variation in the oxidizer can drastically change the combustion process. Although the discrepancy in the temperature profiles between methane ($CH_4$) and ammonia ($NH_3$) flames, the calculated results for $CH_4$ combustion are generally in good agreement with experimentally determined data, demonstrating that the computational model adopted in the present work is sufficiently accurate, and can be also applied to capture ammonia combustion characteristics.

## 3. Results and discussion

### 3.1. Combustion and $NO_x$ emission preliminary results

Firstly, let's examine and compare the combustion and $NO_x$ emission performances in the absence/presence of a perforated plate (PP). Fig. 5 illustrates the NO and temperature contours with overlaid streamlines on the cross section without and with a perforated plate, as the $NH_3$ volumetric flow rate is set to 700 mL/min. Hydroxyl radical (OH) is normally regarded as the marker of the flame front, and, thus, 10% of the maximum OH is chosen to represent the flame shape. As shown in Fig. 5 (a), it can be observed that the flame front and the region with a high concentration of NO reside near the combustor inlet, regardless of with or without a perforated plate. Nevertheless, there is a remarkable difference in the NO concentration downstream of the plate. Specifically, for the combustor with a perforated plate, the NO concentration is much lower than that of without a plate. The reason for this can be explained by comparing the temperature distribution, as illustrated in Fig. 5 (b). From this figure, it can be seen that the implementation of the perforated plate enables a recirculation zone being formed downstream, where the low flame temperature is relatively

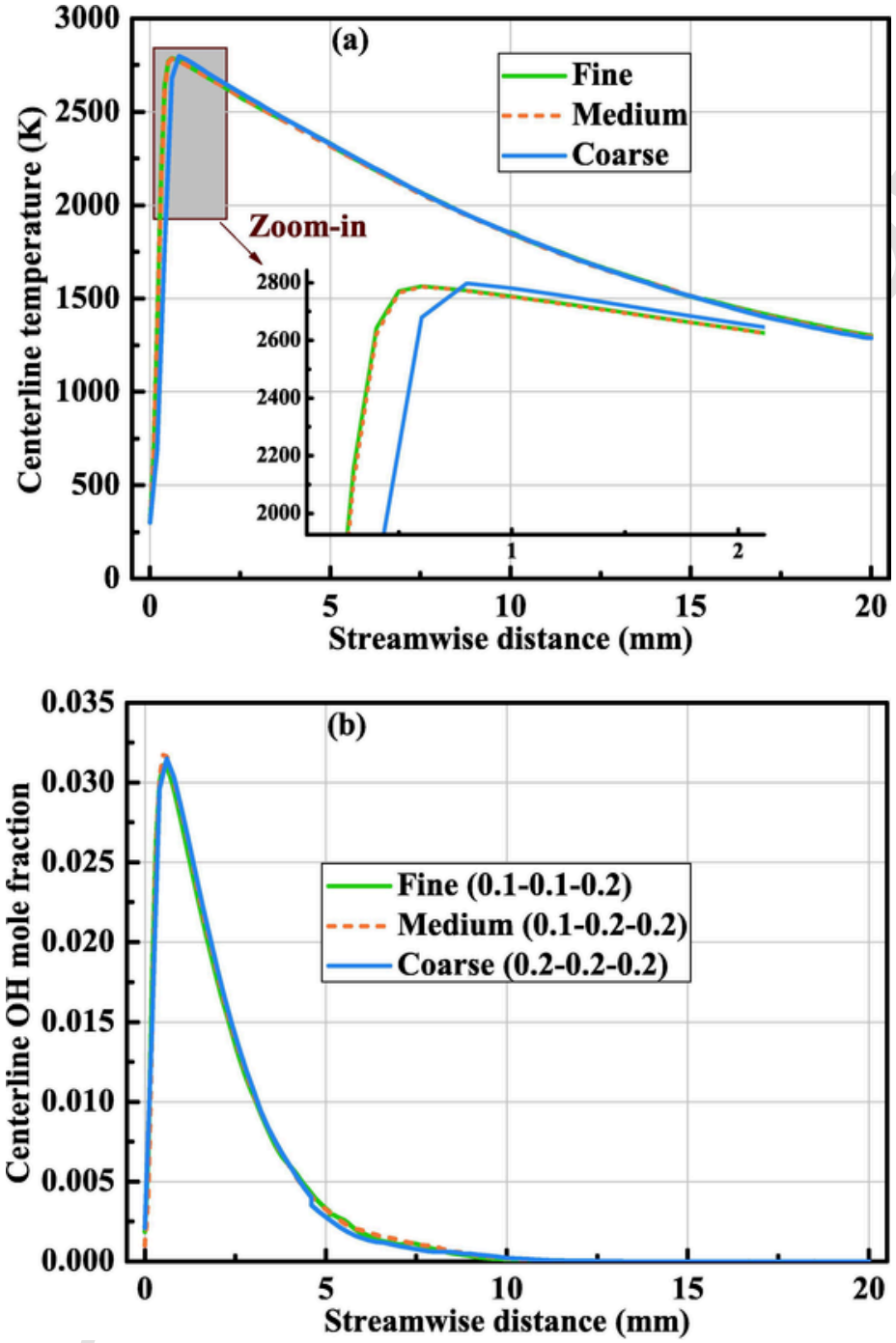


**Fig. 2.** Profiles of (a) temperature and (b) OH radical on the cross-section in the axial direction with the grid cell being set to 3 different values.

lower in comparison to those without a perforated plate. The decreased temperature can be beneficial to reducing the NO generation, as it is highly related to the flame temperature.

To quantify the effect of the perforated plate on the NO generation rate more clearly, we further explore the NO mole fraction on the combustor outlet and reduction ratio with the $NH_3$ volumetric flow rate. This is illustrated in Fig. 6. Herein, the reduction ratio (RR) is given by:

$$RR = \frac{X_{wo} - X_{wt}}{X_{wo}} \times 100\% \quad (2)$$

where RR denotes the reduction ratio of NO mole fraction, $X_{wo}$ and $X_{wt}$ are the NO mole fractions at the combustor outlet in the absence and presence of a perforated plate, respectively.

Fig. 6 shows that in the absence of the perforated plate, there is a slight increase in the NO formation with increasing the $NH_3$ volumetric flow rate. However, this is not the same situation in the presence of the perforated plate, under which condition a decreased NO emission can be observed. This indicates the enhanced effectiveness of implementing a perforated plate with an increased fuel flow rate. These data are consistent with the results shown in Fig. 5, further revealing that implementing a perforated plate could be an effective means to dampen the NO formation. To shed more lights on the variation in NO emissions with a perforated plate implemented, detailed analyses and discussion

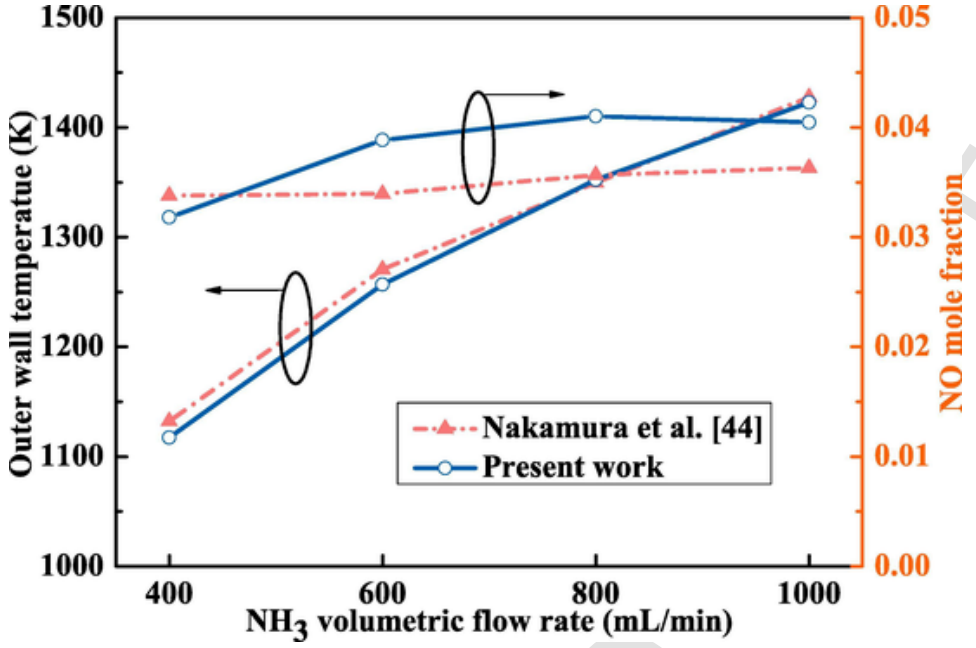


**Fig. 3.** Calculated outer wall temperature and NO mole fraction with the $NH_3$ volumetric flow rate for different chemical-kinetic mechanisms. One is discussed by Nakamura et al. [43], and the other one is developed by Drake and Blint [29].

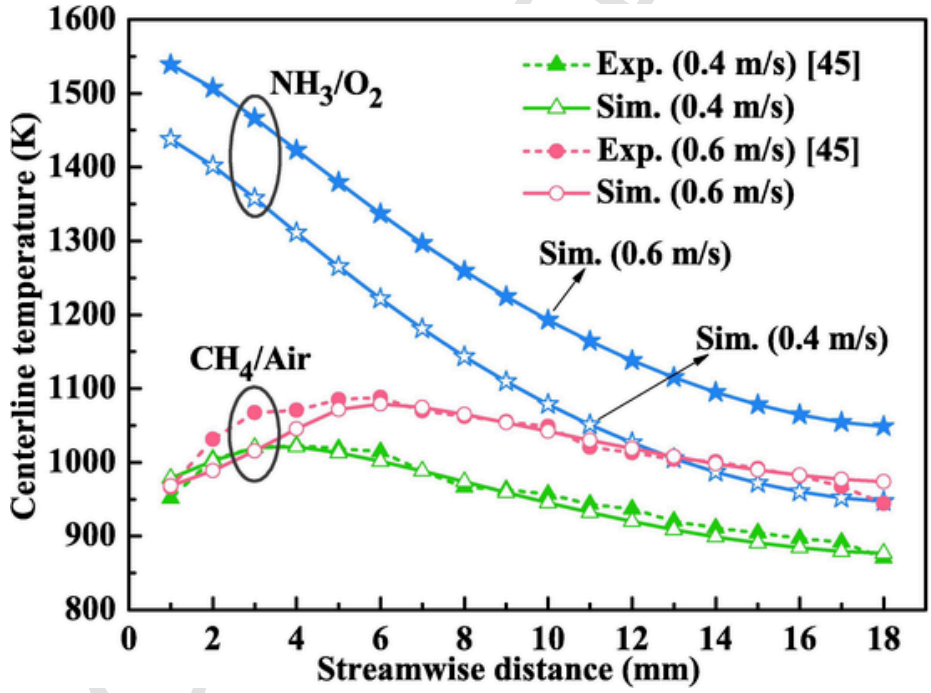


**Fig. 4.** Profiles of calculated and measured centerline temperatures [44] for methane and ammonia flames on the combustor outer wall.

will be conducted in terms of the flow field, the conjugate heat transfer and the preferential diffusion effect in the next section.

### *3.2. Discussion on mechanisms contributing to $NO_x$ formation*

#### *3.2.1. Contribution of recirculation zones to $NO_x$ generation*

Considering that the variation in $\phi$ could lead to the change in the inlet velocity with the fuel volumetric flow rate being kept constant. This change on the circulation flow field and the corresponding decreased temperature is expected to have an important role in the NO formation. Here, we evaluate the effect of flow field on the NO formation. This is achieved by varying the fuel-oxidizer equivalence ratio$\phi$ ranging from 0.8 to 1.0. In this section, the $NH_3$ volumetric flow rate is set to 700 mL/min for all calculations. Fig. 7 illustrates the NO mole fraction contours superimposed by 10% of the maximum OH (blue lines) on the cross-section. It is clear that the flame shape is almost the same anchoring near the combustor inlet, whatever $\phi$ is set to. Moreover, it is interesting to highlight that the NO concentrations vary dramatically with $\phi$. A reduced $\phi$ is found to be associated with a high NO concentration, mainly due to the excess oxygen atoms and OH radical concentration under fuel-lean conditions.

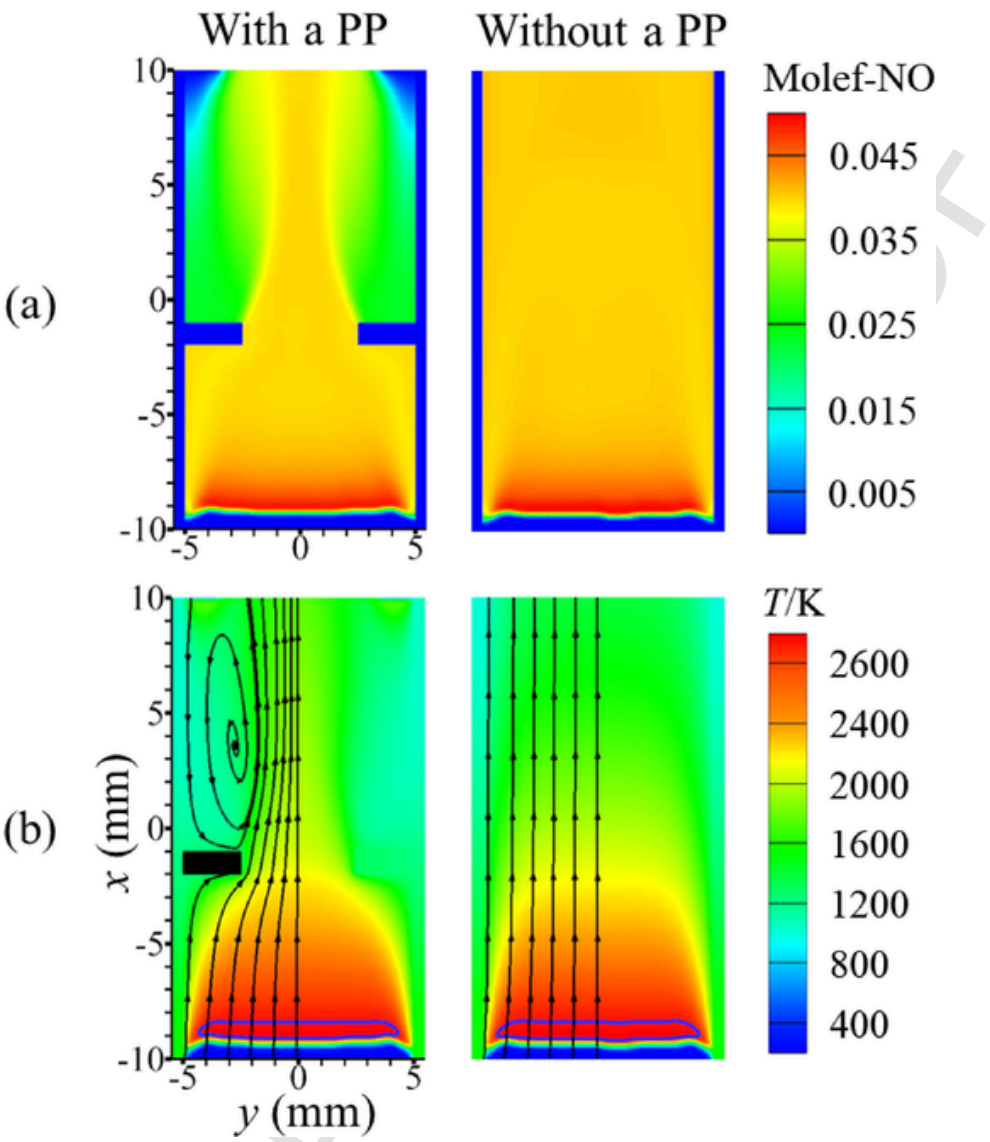


**Fig. 5.** Comparison of (a) NO contours and (b) temperature contour with overlaid streamlines and 10% of the maximum OH (blue lines) on the cross-section in the absence and presence of the perforated plate marked by the black rectangle for the $NH_3$ volumetric flow rate of 700 mL/min. (For interpretation of the references to colour in this figure legend, the reader is referred to the web version of this article.)

Fig. 8 shows the comparison of contours of the flame temperature with overlaid streamlines and velocity field on the cross-section under various $\phi$. From Fig. 8 (a), one can notice that in the presence of the perforated plate, there is a minor difference in the flame temperature, and so is the size of the recirculation zone, regardless of what $\phi$ is specified to. This is because of the same chemical energy input. However, it is worth noting that the decrease in $\phi$ can lead to the maximum flame velocity being increased due to the slightly large mixture inlet velocity, and thus the shortened residence time in the high temperature regions, as shown in Fig. 8 (b). The reduced residence time can be beneficial to mitigating NO emission. However, for ammonia flames, NO formation is highly dependent on the O and OH radicals. Decreasing $\phi$ is found to be associated with a high O and OH concentrations, resulting in a high NO generation [24], as shown in Fig. 7. From Fig. 8 (b), it can be also seen that the flame speed within the recirculation zone is dramatically lower compared to other regions, which is a manifestation of the strong two-dimensionality flow. Comparing Fig. 7 with Fig. 8 shows that the low concentration of NO is located in the recirculation zone, where the flame speed and temperature are relatively low. These results above reveal that the flow field is not the sole factors in determining the total $NO_x$ emissions.

*3.2.2. Effect of conjugate heat transfer*

The results above have an implication that the NO formation may be affected by the coupled heat recirculation effect between the combustion products and the combustor inner walls. This effect has been demonstrated to have a significant impact on the flame shape as well as flame stabilization [45,46]. Thus it would be interesting to know the effect of the conjugate heat transfer between the solid wall and combustion products on the NO formation. For this, three types of materials, namely quartz, steel, and nickel, are chosen to shed light on the underlying physics. The thermophysical properties for three different solid materials are summarized in Table 1.

Fig. 9 presents the NO contours with overlaid streamlines and flame fronts with the fuel flow rate of 700 mL/min at various solid materials. It is clear that for the quartz combustor, the flame anchors just downstream of the plate, accompanied by a high NO concentration, resulting in the deformation of a recirculation zone. This phenomenon is quite different from those with respect to the steel and nickel combus-

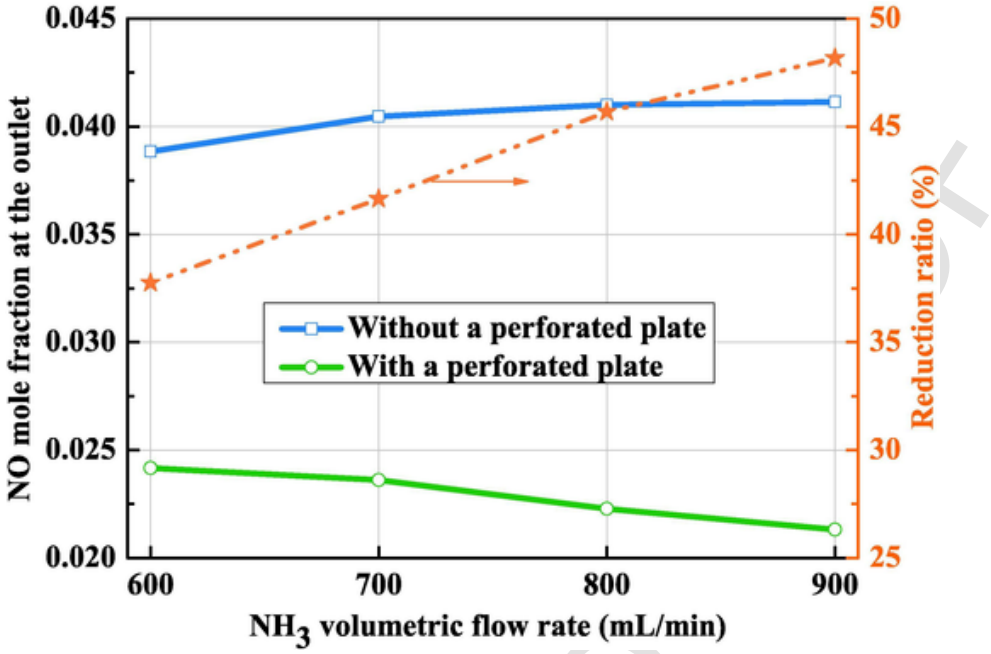


**Fig. 6.** NO mole fractions in the absence and presence of the perforated plate at various $l$ for various $NH_3$ volumetric flow rates.

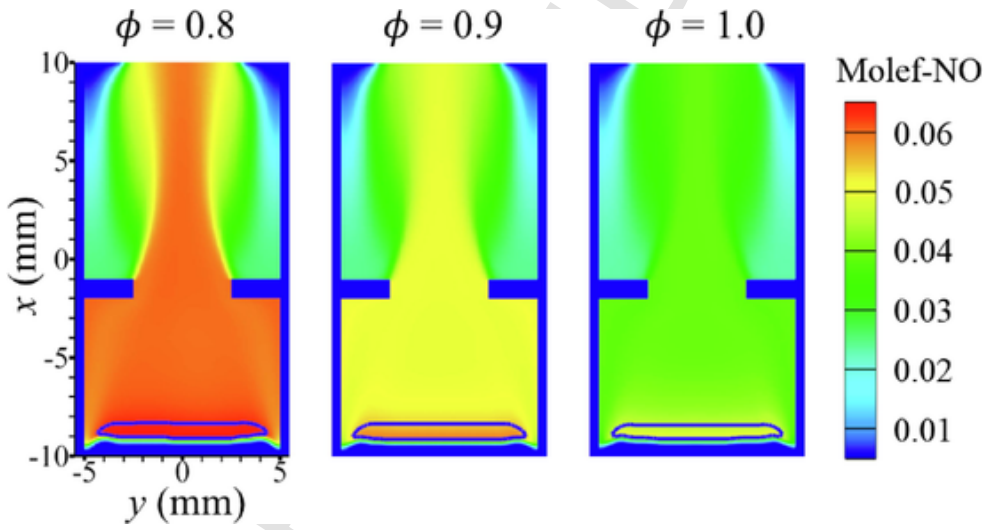


**Fig. 7.** NO mole fraction contours superimposed by 10% of the maximum OH (blue lines) on the cross-section at various $\phi$. (For interpretation of the references to colour in this figure legend, the reader is referred to the web version of this article.)

tors, under which cases the flames occur near the combustor inlet. The reason for this can be understood by comparing the thermal conductivities of the different solid materials. A large thermal conductivity is more effective in transferring the heat between the solid and combustion products. The intensified heat recirculation can enable the flame to propagate upstream and anchor near the combustor inlet. This finding was also confirmed in the previous study [47].

Another noticeable feature shown in Fig. 9 is that as expected, the zone with a high NO concentration is varied dramatically at different solid materials. To be specific, for the quartz combustor with a relatively low thermal conductivity, the high NO concentration appears downstream of the perforated plate, due to the absence of the recirculation zone. In contrast, this zone resides near the combustor inlet for steel and nickel combustors, and the axial location of these zones is negligible. This suggests that when the thermal conductivity of the solid wall reaches a threshold, further increasing this has a slight effect on the conjugate heat transfer and thus flame characteristics. This is mainly due to the well-established recirculation zone downstream of the perforated plate. Moreover, it is worthwhile to highlight that for the quartz combustor, the NO concentration at the combustor outlet is significantly higher than the other two cases. This difference can be attributed to the formation of a recirculation zone capable of providing a low flame temperature.

To reveal the underlying mechanism leading to the variations of the flame shape and NO emission at various solid materials, a further investigation on the centerline temperatures of the combustor inner and outer walls is conducted. This is illustrated in Fig. 10. Solid lines represent the centerline temperatures on the outer wall of the combustor, while the dash lines stand for those on the cross-section of x = 0. From the dash lines, it can be observed that for steel and nickel combustors, the high temperature, generally accompanied by the occurrence of the chemical reaction, is located near the combustor inlet; however, this appears at a distance of up to 10 mm away from the inlet for the quartz combustor. Furthermore, it can be noted from dash lines

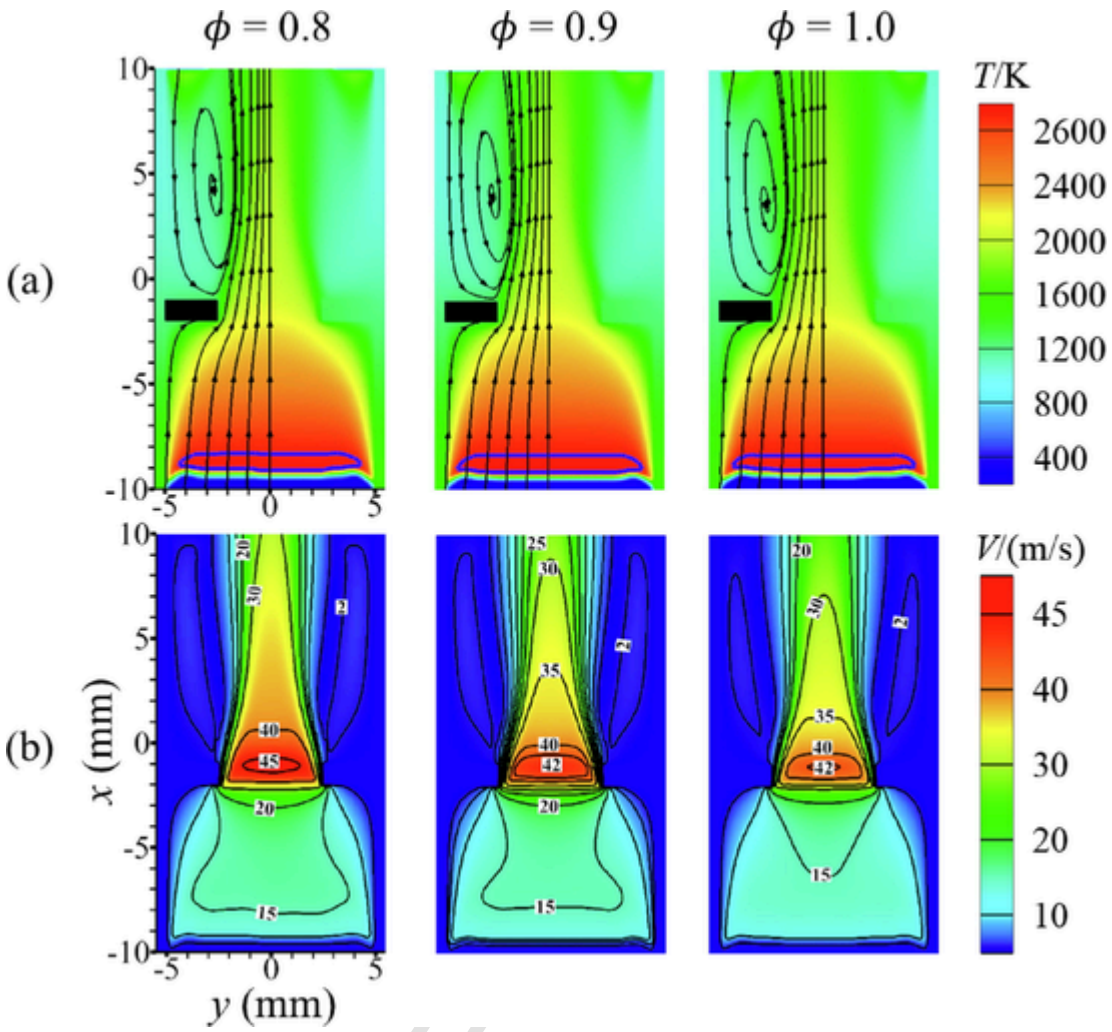


**Fig. 8.** Contours of (a) temperature with overlaid streamlines and 10% of the maximum OH (blue lines), and (b) velocity field on the cross-section at various $\phi$. (For interpretation of the references to colour in this figure legend, the reader is referred to the web version of this article.)

**Table 1**
Thermophysical properties of quartz, steel and nickel.

| Material | Density kg/m$^3$ | Specific Heat J/kg·K | Thermal Conductivity $W/m{\cdot}K$ | Emissivity |
|---|---|---|---|---|
| Quartz | 2650 | 750 | 1.05 | 0.92 |
| Steel | 8000 | 503 | 12 | 0.85 |
| Nickel | 8900 | 460.6 | 91.74 | 0.88 |

that the centerline temperature of the quartz combustor is much steeper in comparison with others, which is a manifestation of the weak heat transfer between solid walls and combustion products, and further demonstrating that the solid material plays a critical role in the flame location and shape. A comparison of Figs. 9 and 10 shows that the solid material plays a vital role in the $NO_x$ emissions by affecting the flame characteristics and thus the formation of a recirculation zone.

*3.2.3. Contribution of preferential diffusion mechanism to $NO_x$ formation*

In addition to the physical mechanisms contributing to the NO emission variation as discussed above, it is of particular interest to consider the impact of the preferential diffusion effect, which is expected to occur due to the imbalance in the mass diffusivities of different species, and can be amplified by the presence of a recirculation zone. This phenomenon was experimentally demonstrated by Barlow and co-workers [48,49] in a bluff-body stabilized flames using multiscalar diagnostics. They pointed out that the existence of preferential diffusion effect could result in more than 10% increase in the equivalence ratio and the carbon-to-hydrogen atom ratio. This variation in the different atom ratios was subsequently confirmed by Katta and Roquemore [50], as well as Kedia and Ghoniem [46] in the context of a recirculation zone using numerical simulations. To examine the role of preferential diffusion in NO formation, we define a local nitrogen-to-oxygen atomic ratio ($\gamma_{N/O}$) and nitrogen-to-hydrogen atomic ratio ($\gamma_{N/H}$) on the basis of the local atoms balance using major species associated with the formation and destruction of nitrogen oxides. The formulas of $\gamma_{N/O}$ and $\gamma_{N/H}$ are expressed as follows:

$$\gamma_{N/O} = \frac{X_{N_2} + X_{N_2O} + 0.5(X_N + X_{NO} + X_{NO_2} + X_{NH_3})}{X_{O_2} + X_{NO_2} + 0.5(X_O + X_{OH} + X_{NO} + X_{H_2O} + X_{N_2O})} \quad (3)$$

$$\gamma_{N/H} = \frac{X_N + X_{NO} + X_{NO_2} + X_{NH_3} + 2(X_{N_2} + X_{N_2O})}{X_H + X_{OH} + 2(X_{H_2} + X_{H_2O}) + 3X_{NH_3}} \quad (4)$$

where $X_i$ denotes the mole fraction of species *i*. The local equivalence ratio ($\phi_{local}$) can be calculated according to:

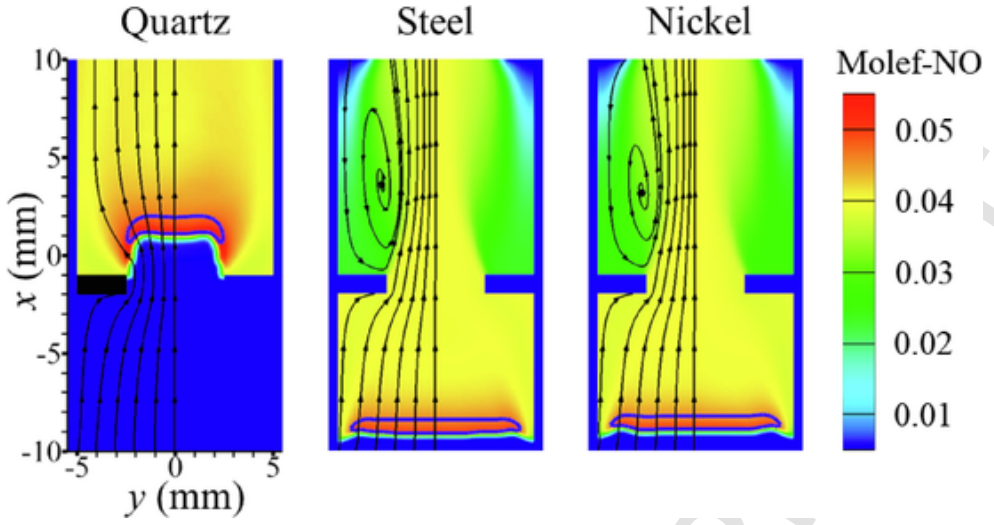


**Fig. 9.** NO contours with overlaid streamlines and normalized of 10% of the maximum OH radicals on the cross-section for 3 different solid materials.

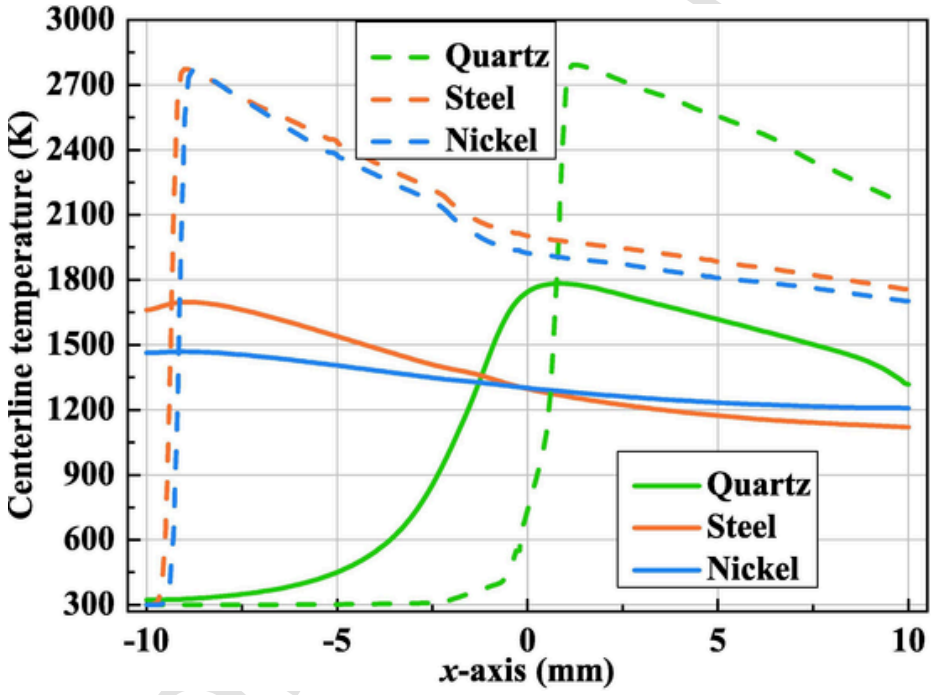


**Fig. 10.** Profiles of centerline temperatures on the inner wall and outer wall for 3 different thermal conductivities of the combustor. Solid lines represent the centerline temperatures on the outer wall of the combustor, while the dash lines stand for those on the cross-section.

$$\phi_{local} = \frac{0.25\left(X_H + X_{OH}\right) + 0.5\left(X_{H_2} + X_{H_2O}\right) + 0.75X_{NH_3}}{X_{O_2} + X_{NO_2} + 0.5(X_O + X_{OH} + X_{NO} + X_{H_2O} + X_{N_2O})} \quad (5)$$

With respect to ammonia flames under the stoichiometric condition, $\gamma_{N/O} = 2/3$, and $\gamma_{N/H} = 1/3$. Certainly, these atomic ratios may change with the initial fuel/oxidizer equivalence ratio, except for the N/H atomic ratio remaining unchanged, since these two types of atoms are initially from $NH_3$. Thus, the local atomic ratio can be regarded as an indicator of how much influence the preferential diffusion effect plays on the combustion process. Table 2 summarizes the local equivalence ratio, atomic ratios, and the rise above the initial ratio for various equivalence ratios, as the $NH_3$ volumetric flow rate is set to 700 mL/min. It can be observed that there are some differences between the initial value and local atomic ratio, no matter which equivalence ratio is set to, implying the existence of the preferential diffusion effect.

**Table 2**
The maximum atomic ratios and $\phi_{local}$ at different $\phi$, with the $NH_3$ volumetric flow rate being set to 700 mL/min.

| $\phi$ | Maximum $\phi_{local}$ (rise above initial ratio) | Maximum $\gamma_{N/O}$ (rise above initial ratio) | Maximum $\gamma_{N/H}$ (rise above initial ratio) |
|---|---|---|---|
| 0.8 | 0.832 (+5.2%) | 0.555 (+4.1%) | 0.344 (+3.7%) |
| 0.9 | 0.939 (+4.3%) | 0.622 (+3.7%) | 0.346 (+3.8%) |
| 1.0 | 1.052 (+3.9%) | 0.686 (+2.9%) | 0.346 (+3.3%) |

To illuminate the preferential diffusion effect more clearly, the contours of the N/H atomic ratio $\gamma_{N/H}$ overlaid with NO mole fraction using a steel combustor are investigated, as presented in Fig. 11. From

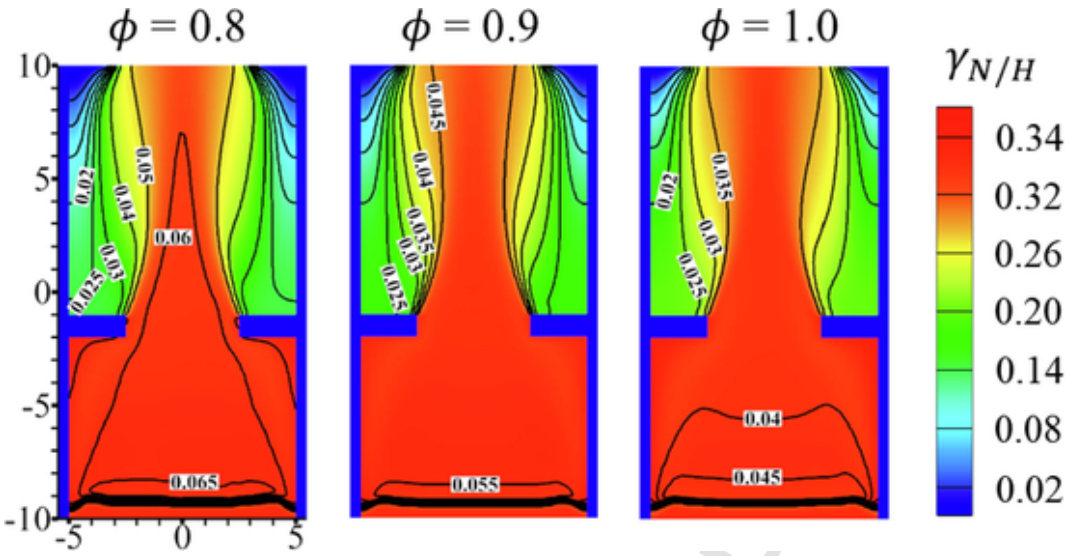


**Fig. 11.** Contours of the local N/H atomic ratio overlaid with NO mole fraction with the fuel flow rate being set to 700 mL/min using a steel combustor.

this figure, it can be seen that the maximum value of $\gamma_{N/H}$ anchors near the combustor inlet, no matter which the initial equivalence ratio is set to, suggesting that the preferential diffusion of different species is not just limited within the recirculation zone. Meanwhile, it can also be observed that there are significant drops in the $\gamma_{N/H}$ within the recirculation zone, accompanied by a low NO concentration, which is a demonstration of the strong preferential diffusion effect caused by the two-dimensionality flow. In addition, a close examination of Fig. 11 shows that there are some differences in $\gamma_{N/H}$ for different equivalence ratios, indicating that the preferential diffusion is dependent on the local flow field.

In view of the atomic preferential diffusion for different fuel/oxidizer equivalence ratios discussed above, it would also be interesting to explore if the solid material has the similar effect. This is done by comparing the contours of $\phi_{local} - \phi$ superimposed by NO mole fraction with three types of solid materials, as the $NH_3$ volumetric flow rate is set to 700 mL/min, as shown in Fig. 12. For the quartz combustor, there is a small change of $\phi_{local} - \phi$ in the regions near and far from the perforated plate, mainly due to the absence of the recirculation zone. On the contrary, the change is significant for steel and nickel combustors. This change is quite understandable as a result of the well-established recirculation zone downstream of the perforated plate, inside which the preferential diffusion is intensive because of the strong two-dimensionality flow. Generally, the value of $\phi_{local} - \phi$ within the recirculation zone is relatively smaller, which is a manifestation of the strong preferential diffusion effect.

Fig. 13 illustrates the comparison of the predicted profiles of the atomic ratios and local equivalence ratio along the *y*-axis at different $\Delta x$. Hereafter, $\Delta x$ represents the distance away from the downstream face of the perforated plate in the streamwise direction. It can be seen from the figure that the atomic ratios and local equivalence ratio profiles are almost similar in the shape for different $\Delta x$, with high values close to the initial ratio in the center of *y*-axis and low values away from the center. However, they vary quantitatively to some extent. This is because when the flame is in the middle of *y*-axis, it is outside the recirculation zone and the two-dimensionality flow effect is weak, thus resulting in the weak preferential diffusion. Another striking feature shown in Fig. 13 is that there are low atomic ratios even at a far distance such as $\Delta x = 12\,t$, suggesting that the preferential diffusion is not limited to the flame within the recirculation zone. Furthermore, it should be pointed out that when the flame is far away from the center of *y*-axis, the preferential diffusion effect appears to change signifi-

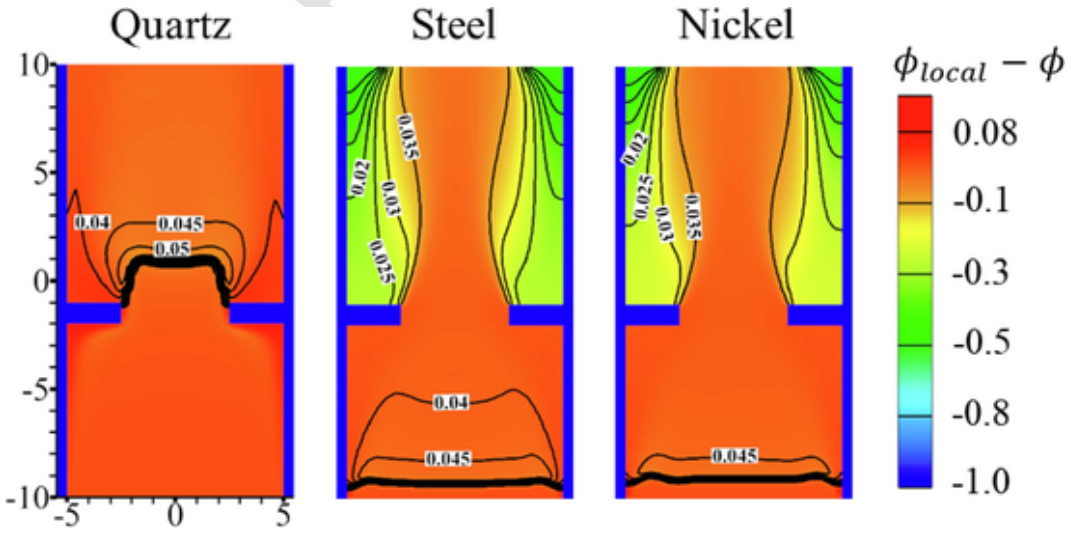


**Fig. 12.** Contours of $\phi_{local} - \phi$(the departure of local fuel/oxidizer equivalence ratio from the initial one) overlaid with NO mole fraction for various solid materials.

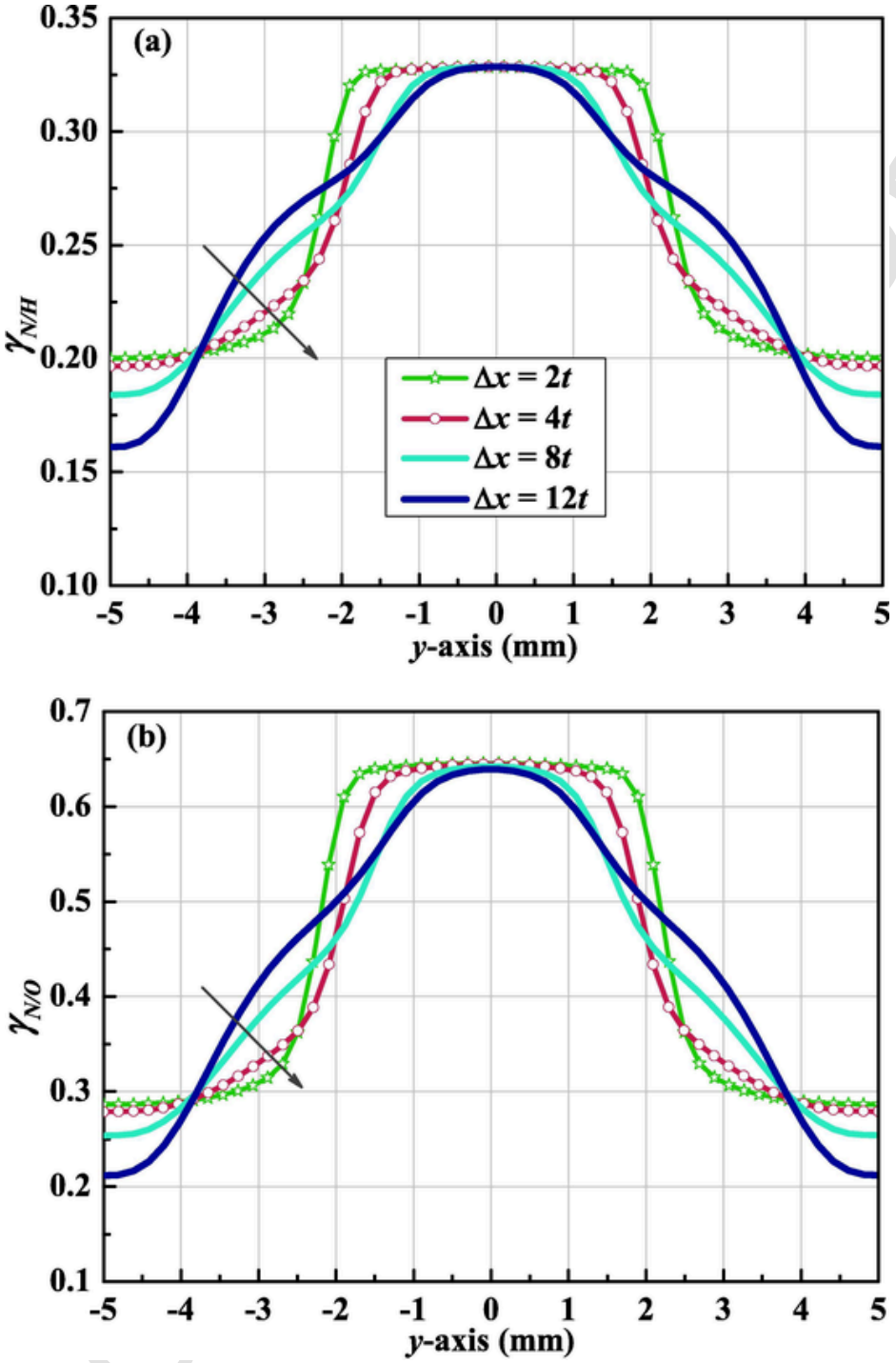


**Fig. 13.** Profiles of atomic ratios and local equivalence ratio along the *y*-axis at distances of 2 *t*, 4 *t*, 8 *t* and 12 *t* using a steel combustor. The arrow is in direction of decreasing the distance from the perforated plate.

cantly with $\Delta x$. For example, at $y = -5$ mm, increasing $\Delta x$ is found to be associated with an enhanced preferential effect. In general, the local atomic ratio and equivalence ratio within the recirculation zone are smaller than the initial value, primarily due to the strong preferential diffusion effect.

Further insight into the preferential effect within the recirculation zone can be gained by examining the major species distribution [51]. Fig. 14 presents the comparison of contours of major species including $N_2$, $O_2$, $H_2$, and $H_2O$ on the cross-section in the presence/absence of the perforated plate, with the $NH_3$ volumetric flow rate being set to 700 mL/min. It is apparent that in the presence of the perforated plate, the major species concentrations within the recirculation zone are dramatically different from those in the absence of the perforated plate. Comparing Fig. 14 (a), (b), and (c) shows that the increase of H atom mainly coming from $H_2$ and $H_2O$ due to combustion products recirculation is negligible, while there are some drops in $N_2$ concentrations, resulting in the drop of $\gamma_{N/H}$·It therefore reveals that increased $N_2$ is the main reason for the varied N/H atomic ratio. Regarding the decrease in $\gamma_{N/O}$, its underlying mechanism can be obtained by comparing Fig. 14 (a), (b), and (d). For the combustor with the perforated plate, there are

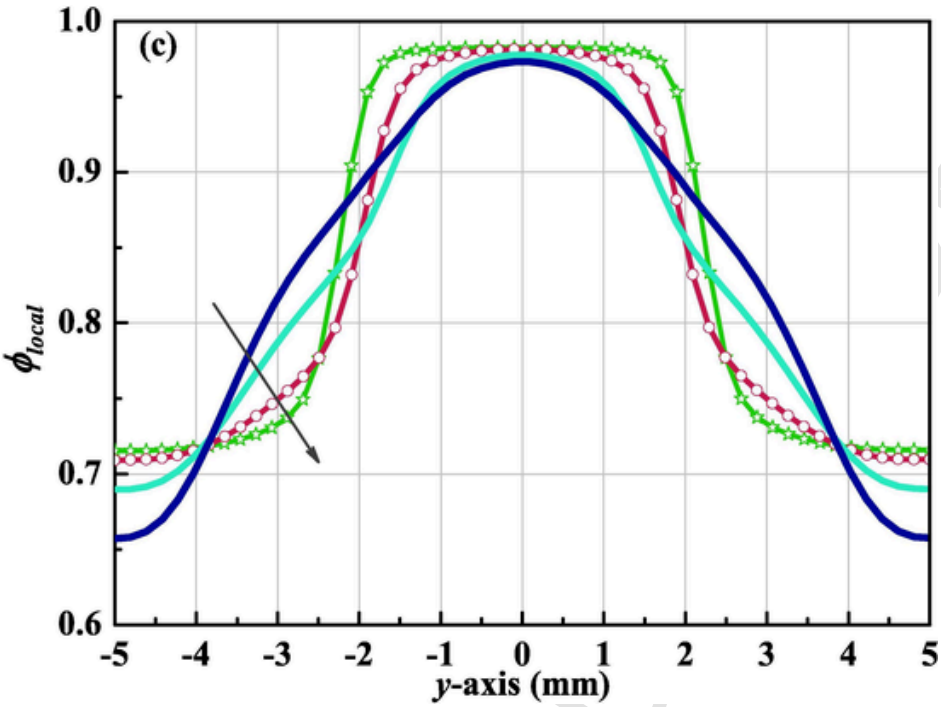


Fig. 13. *Continued*

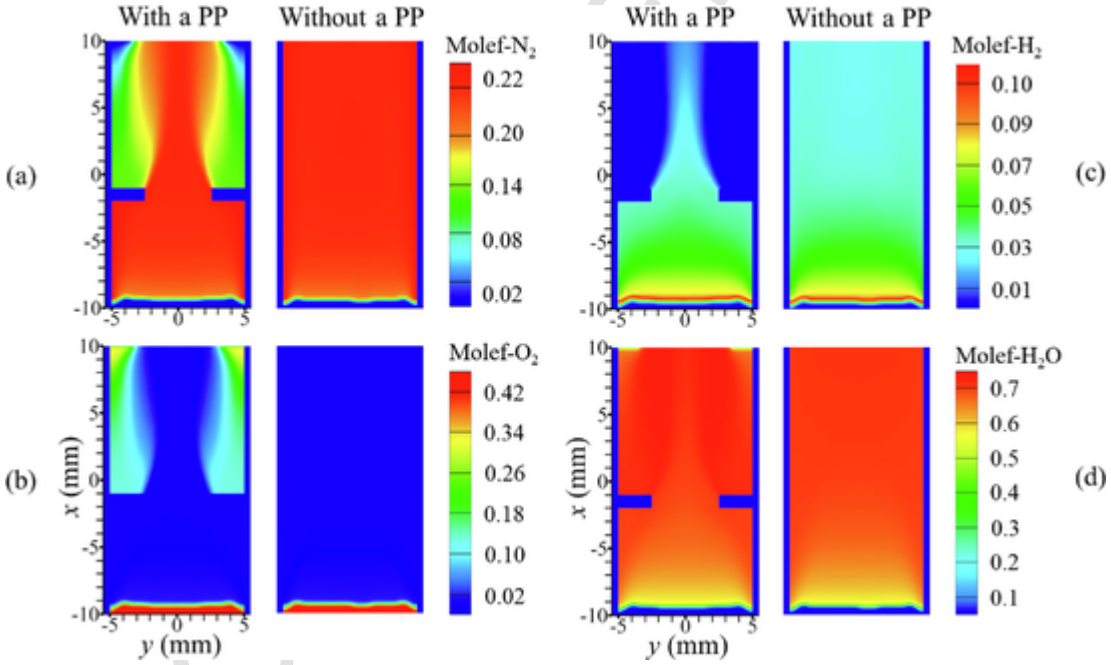


**Fig. 14.** Comparison of distributions of major species: (a) $N_2$, (b) $O_2$, (c) $H_2$, and (d) $H_2O$ on the cross-section in the presence/ absence of the perforated plate using a steel combustor, as the $NH_3$ volumetric flow rate is set to 700 mL/min.

some accumulations of O and drops of N within the recirculation zone in comparison to the case in the absence of the perforated plate, indicating that the accumulation of $O_2$ and $H_2O$, together with less available $N_2$, plays a critical role in the N/O ratio. Furthermore, a close examination of Fig. 14 (b), (c), and (d) shows that the accumulation of $O_2$ in the recirculation zone is the major cause for the variation in the atomic ratio. Therefore, it can be inferred that the preferential diffusion has an effect on the $NO_x$ emissions within the recirculation zone, mostly as a result of combustion products recirculation and the difference in the mass diffusivities of different species.

To further evaluate the degree of the mass transport inside the micro-combustor, we introduce a dimensionless group, the local Peclet number. This dimensionless number represents the relative importance of convection to diffusion mass transfer, which is calculated as follows:

$$\mathrm{Pe} = \frac{u \times \rho \times C_p \times D}{k}$$

where $u$ stands for the fluid velocity (m/s), $\rho$ stands for the density $\left(\mathrm{kg/m^3}\right)$, $C_p$ represents the specific heat of species (J/(kg·K), $D$ repre-

sents the characteristic length of the flow ($m$), and $k$ is the thermal conductivity (W/(m·K)).

Fig. 15 compares the Peclet number with the distance along the $y$-axis in the absence/presence of a perforated plate. It is noted that the Peclet number tends to be higher in the center of the axis, and lower close to the inner walls, regardless of whether a perforated plate is implemented or not. It is, however, worth highlighting that in the presence of the perforated plate, the Peclet number close to the inner walls is significantly lower compared to those without a perforated plate. This reveals the strong diffusion effect within the recirculation zone.

## 4. Conclusions

In this work, the $NO_x$ emission performances of ammonia/oxygen combustion in a perforated plate-implemented micro-combustor are numerically explored by considering the contributions of the flow field, conjugate heat transfer as well as preferential diffusion effects. For this, a 3D computational model with detailed chemical-kinetic mechanisms is developed and validated by comparing with the experimental data available in the literature. It is found that the compared to those without a perforated plate, the presence of the perforated plate can reduce temperature/flame speed, which contribute to $NO_x$ variation in the recirculation zones. Detailed analyses reveal that implementing a perforated plate enables a recirculation zone being formed downstream of the plate. This zone, characterized by a low flame speed and temperature, is found to play an important role in changing the flow field. In addition, the conjugate heat transfer between combustion products and solid walls is identified to have a considerable effect on the NO generation by relocating the flame and thus affecting chemical reactions. Finally, the preferential transport effect caused by the difference in the mass diffusivity of different species and the two-dimensionality flow is identified, leading to a region of locally decreased equivalence ratio and atomic ratios. A significant decrease in N/O atomic ratio is observed in the recirculation zone, mainly due to the increase of O atoms, together with less N atoms available. This contributes to the change in the NO generation in the recirculation zones.

In general, the present work proposes and examines a new design of micro-combustion systems by implementing a perforated plate. Furthermore, the flow field, the conjugate heat transfer as well as the preferential diffusion mechanisms are identified to affect $NO_x$ emissions in the recirculation zones to some extent from a perforated plate-applied micro-combustor.

## Declaration of Competing Interest

The authors declare that they have no known competing financial interests or personal relationships that could have appeared to influence the work reported in this paper.

## Acknowledgements

We gratefully acknowledge the financial support provided by the University of Canterbury, New Zealand (grant no. CPS20-03-002) and National Research Foundation Singapore (grant no. NRF2016 NRF-NSFC001-102). Tao Cai would like to thank to College of Engineering, University of Canterbury for providing PhD studentship.



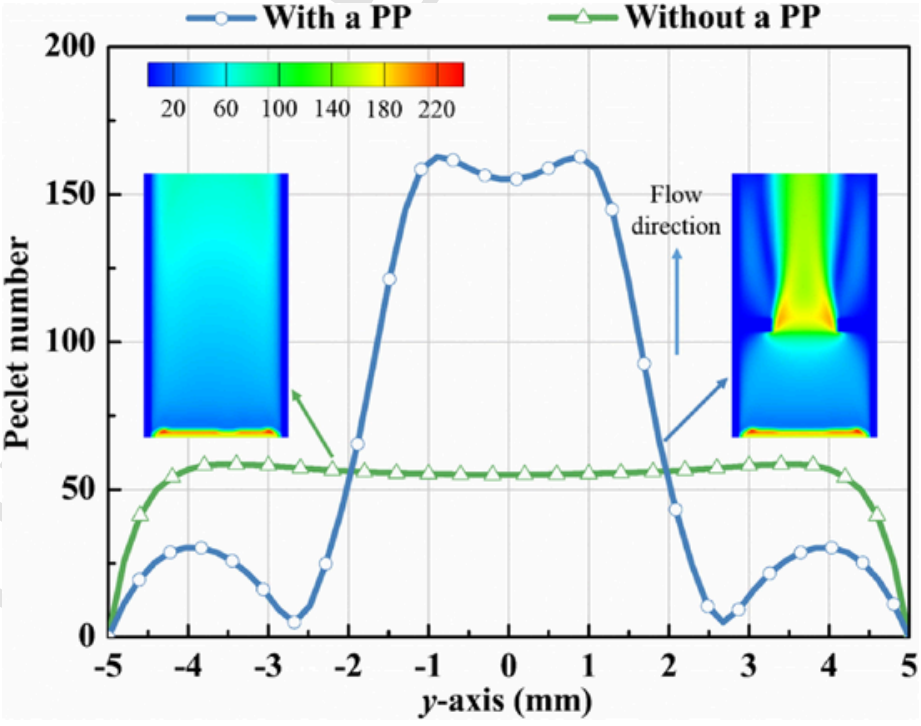


**Fig. 15.** Variation of Peclet number along the $y$-axis with and without a perforated plate implemented.

## References


[1] A. Valera-Medina, H. Xiao, M. Owen-Jones, W.I.F. David, P.J. Bowen, Ammonia for power, Prog. Energy Combust. Sci. 69 (2018) 63–102.
[2] H. Kobayashi, A. Hayakawa, K.D.K.A. Somarathne, E.C. Okafor, Science and technology of ammonia combustion, Proc. Combust. Inst. 37 (1) (2019) 109–133.
[3] C. Zamfirescu, I. Dincer, Using ammonia as a sustainable fuel, J. Power Sources 185 (1) (2008) 459–465.
[4] S. Verhelst, T. Wallner, Hydrogen-fueled internal combustion engines, Prog. Energy Combust. Sci. 35 (6) (2009) 490–527.
[5] J. Li, H.Y. Huang, N. Kobayashi, Z.H. He, Y. Nagai, Study on using hydrogen and ammonia as fuels: Combustion characteristics and NOx formation, Int. J. Energy Res. 38 (9) (2014) 1214–1223.
[6] K. Takizawa, A. Takahashi, K. Tokuhashi, S. Kondo, A. Sekiya, Burning velocity measurements of nitrogen-containing compounds, J. Hazard. Mater. 155 (1–2) (2008) 144–152.
[7] R.F. Service, Ammonia-a renewable fuel made from sun, air, and water-could power the globe without carbon. Science (2018) http://10.1126/science.aau7489.
[8] R. Michalsky, B.J. Parman, V. Amanor-Boadu, P.H. Pfromm, Solar thermochemical production of ammonia from water, air and sunlight: Thermodynamic and economic analyses, Energy 42 (1) (2012) 251–260.
[9] C. Lhuillier, P. Brequigny, N. Lamoureux, F. Contino, C. Mounaïm-Rousselle, Experimental investigation on laminar burning velocities of ammonia/hydrogen/air mixtures at elevated temperatures, Fuel 263 (2020), doi:10.1016/j.fuel.2019.116653.
[10] Q.M. Liu, X. Chen, J.X. Huang, Y. Shen, Y.M. Zhang, Z.W. Liu, The characteristics of flame propagation in ammonia/oxygen mixtures, J. Hazard. Mater. 363 (2019) 187–196.
[11] A. Hayakawa, T. Goto, R. Mimoto, Y. Arakawa, T. Kudo, H. Kobayashi, Laminar burning velocity and Markstein length of ammonia/air premixed flames at various pressures, Fuel 159 (2015) 98–106.
[12] H. Nakamura, M. Shindo, Effects of radiation heat loss on laminar premixed ammonia/air flames, Proc. Combust. Inst. 37 (2) (2019) 1741–1748.
[13] A. Hayakawa, Y. Arakawa, R. Mimoto, K.D. Kunkuma, A. Somarathne, T. Kudo, H. Kobayashi, Experimental investigation of stabilization and emission characteristics of ammonia/air premixed flames in a swirl combustor, Int. J. Hydrogen Energy 42 (19) (2017) 14010–14018.
[14] H. Xiao, A. Valera-Medina, P.J. Bowen, Study on premixed combustion characteristics of co-firing ammonia/methane fuels, Energy 140 (2017) 125–135.
[15] A. Valera-Medina, R. Marsh, J. Runyon, D. Pugh, P. Beasley, T. Hughes, P. Bowen, Ammonia-methane combustion in tangential swirl burners for gas turbine power generation, Appl. Energy 185 (2017) 1362–1371.
[16] A. Valera-Medina, D.G. Pugh, P. Marsh, G. Bulat, P. Bowen, Preliminary study on lean premixed combustion of ammonia-hydrogen for swirling gas turbine combustors, Int. J. Hydrogen Energy 42 (38) (2017) 24495–24503.
[17] E.C. Okafor, K.D.K.A. Somarathne, A. Kunkuma, A. Hayakawa, T. Kudo, O. Kurata, N. Iki, H. Kobayashi, Towards the development of an efficient low-NOx ammonia combustor for a micro gas turbine, Proc. Combust. Inst. 37 (4) (2019) 4597–4606.
[18] Y. Wang, Y.X. Liu, S. Shi, Removal of nitric oxide from flue gas using novel microwave-activated double oxidants system, Chem. Eng. J. 393 (2020), doi:10.1016/j.cej.2020.124754.
[19] Y. Wang, Y.X. Liu, Y. Liu, Elimination of nitric oxide using new Fenton process based on synergistic catalysis: Optimization and mechanism, Chem. Eng. J. 372 (2019) 92–98.
[20] T. Cai, D. Zhao, E. Jiaqiang, Bluff-body effect on thermal and NOx emission characteristics in a micro-planar combustor fueled with premixed ammonia-oxygen, Chem. Eng. Process: Process Intensif. 153 (2020), doi:10.1016/j.cep.2020.107979.
[21] A.M. Elbaz, H.A. Moneib, K.M. Shebil, W.L. Roberts, Low $NO_X$ - LPG staged combustion double swirl flames, Renew. Energy 138 (2019) 303–315.
[22] K.D.K.A. Somarathne, E.C. Okafor, A. Hayakawa, T. Kudo, O. Kurata, N. Iki, H. Kobayashi, Emission characteristics of turbulent non-premixed ammonia/air and methane/air swirl flames through a rich-lean combustor under various wall thermal boundary conditions at high pressure, Combust. Flame 210 (2019) 247–261.
[23] K.D.K.A. Somarathne, S. Colson, A. Hayakawa, H. Kobayashi, Modelling of ammonia/air non-premixed turbulent swirling flames in a gas turbine-like combustor at various pressures, Combust. Theory Modell. 22 (5) (2018) 973–997.
[24] T. Cai, D. Zhao, B. Wang, J.W. Li, Y.H. Guan, $NO_x$ emission and thermal performances studies on premixed ammonia-oxygen combustion in a $CO_2$-free micro-planar combustor, Fuel 280 (2020), doi:10.1016/j.fuel.2020.118554.
[25] E.C. Okafor, K.D.K.A. Somarathne, R. Ratthanan, A. Hayakawa, T. Kudo, O. Kurata, N. Iki, T. Tsujimura, H. Furutani, H. Kobayashi, Control of NOx and other emissions in micro gas turbine combustors fuelled with mixtures of methane and ammonia, Combust. Flame 211 (2020) 406–416.
[26] T. Meyer, P. Kumar, M. Li, K. Redfern, D. Diaz, Ammonia combustion with near-zero pollutant emissions. (2011) NH3 fuel association. NH3 Congress, Iowa, USA, 2011.
[27] K.D.K.A. Somarathne, S. Hatakeyama, A. Hayakawa, H. Kobayashi, Numerical study of a low emission gas turbine like combustor for turbulent ammonia/air premixed swirl flames with a secondary air injection at high pressure, Int. J. Hydrogen Energy 42 (44) (2017) 27388–27399.
[28] T. Cai, D. Zhao, Effects of fuel composition and wall thermal conductivity on thermal and $NO_x$ emission performances of an ammonia/hydrogen-oxygen micro-power system, Fuel Process. Technol. 209 (2020), doi:10.1016/j.fuproc.2020.106527.
[29] M.C. Drake, R.J. Blint, Thermal $NO_x$ in stretched laminar opposed-flow diffusion flames with $CO/H_2/N_2$ fuel, Combust. Flame 76 (1989) 151–167.
[30] C.H. Kuo, P.D. Ronney, Numerical modeling of non-adiabatic heat-recirculating combustors, Proc. Combust. Inst. 31 (2) (2007) 3277–3284.
[31] ANSYS Fluent User's Guide, Release 18.1, ANSYS, Inc., April 2017.
[32] L.H. Li, S.X. Wang, L. Zhao, A.W. Fan, A numerical investigation on non-premixed catalytic combustion of $CH_4/(O_2 + N_2)$ in a planar micro-combustor, Fuel 255 (2019), doi:10.1016/j.fuel.2019.115823.
[33] H. Bongers, L.P.H. De Goey, The effect of simplified transport modeling on the burning velocity of laminar premixed flames, Combust. Sci. Technol. 175 (10) (2003) 1915–1928.
[34] W.M. Yang, D.Y. Jiang, K.Y.K. Chua, D. Zhao, J.F. Pan, Combustion process and entropy generation in a novel microcombustor with a block insert, Chem. Eng. J. 274 (2015) 231–237.
[35] W.M. Yang, K.J. Chua, J.F. Pan, D.Y. Jiang, H. An, Development of micro-thermophotovoltaic power generator with heat recuperation, Energy Convers. Manage. 78 (2014) 81–87.
[36] W. Zuo, E. Jiaqiang, H.L. Liu, Q.G. Peng, X.H. Zhao, Z.Q. Zhang, Numerical investigations on an improved micro-cylindrical combustor with rectangular rib for enhancing heat transfer, Appl. Energy 184 (2016) 77–87.
[37] P. Glarborg, J.A. Miller, B. Ruscic, S.J. Klippenstein, Modeling nitrogen chemistry in combustion, Prog. Energy Combust. Sci. 67 (2018) 31–68.
[38] G.J. Rortveit, J.E. Hustad, S.C. Li, F.A. Williams, Effects of diluents on $NO_x$ formation in hydrogen counter-flow flames, Combust. Flame 130 (2002) 48–61.
[39] J.L. Wan, A.W. Fan, H. Yao, W. Liu, Flame-anchoring mechanisms of a micro cavity-combustor for premixed $H_2$/air flame, Chem. Eng. J. 275 (2015) 17–26.
[40] W.M. Yang, S.K. Chou, K.J. Chua, J. Li, X. Zhao, Research on modular micro combustor-radiator with and without porous media, Chem. Eng. J. 168 (2) (2011) 799–802.
[41] W. Zuo, E. Jiaqiang, R.M. Lin, Y. Jin, D.D. Han, Numerical investigations on an improved counterflow double-channel micro combustor fueled with hydrogen for enhancing thermal performance, Energy Convers. Manage 159 (2018) 163–174.
[42] W. Zuo, E. Jiaqiang, R.M. Lin, Y. Jin, D.D. Han, Numerical investigations on different configurations of a four-channel meso-scale planar combustor fueled by hydrogen/air mixture, Energy Convers. Manage 160 (2018) 1–13.
[43] H. Nakamura, S. Hasegawa, T. Tezuka, Kinetic modeling of ammonia/air weak flames in a micro flow reactor with a controlled temperature profile, Combust. Flame 185 (2017) 16–27.
[44] A.K. Tang, Y. Xu, J.F. Pan, W.M. Yang, D.Y. Jiang, Q.B. Lu, Combustion characteristics and performance evaluation of premixed methane/air with hydrogen addition in a micro-planar combustor, Chem. Eng. Sci. 131 (2015) 235–242.
[45] J.L. Wan, A.W. Fan, Y. Liu, H. Yao, W. Liu, X.L. Gou, D.Q. Zhao, Experimental investigation and numerical analysis on flame stabilization of $CH_4$/air mixture in a mesoscale channel with wall cavities, Combust. Flame 162 (4) (2015) 1035–1045.
[46] K.S. Kedia, A.F. Ghoniem, The anchoring mechanism of a bluff-body stabilized laminar premixed flame, Combust. Flame 161 (9) (2014) 2327–2339.
[47] T. Cai, A.K. Tang, D. Zhao, C. Zhou, Q.H. Huang, Flame dynamics and stability of premixed methane/air in micro-planar quartz combustors, Energy 193 (2020), doi:10.1016/j.energy.2019.116767.
[48] R.S. Barlow, M.J. Dunn, M.S. Sweeney, S. Hochgreb, Effects of preferential transport in turbulent bluff-body-stabilized lean premixed $CH_4$/air flames, Combust. Flame 159 (8) (2012) 2563–2575.
[49] M.J. Dunn, R.S. Barlow, Effects of preferential transport and strain in bluff body stabilized lean and rich premixed $CH_4$/air flames, Proc. Combust. Inst. 34 (1) (2013) 1411–1419.
[50] V. Katta, W.M. Roquemore, C/H atom ratio in recirculation-zone-supported premixed and nonpremixed flames, Proc. Combust. Inst. 34 (1) (2013) 1101–1108.
[51] D. Michaels, A.F. Ghoniem, Impact of the bluff-body material on the flame leading edge structure and flame-flow interaction of premixed $CH_4$/air flames, Combust. Flame 172 (2016) 62–78.